Investigation of acceleration effects on missile aerodynamics using Computational Fluid Dynamics

I.M.A. Gledhill, K. Forsberg, P. Eliasson, J. Baloyi, J. Nordström

PII: S1270-9638(09)00014-5
DOI: 10.1016/j.ast.2009.04.008
Reference: AESCTE 2446

To appear in: *Aerospace Science and Technology*

Received date: 24 November 2007
Accepted date: 22 April 2009

Please cite this article as: I.M.A. Gledhill, K. Forsberg, P. Eliasson, J. Baloyi, J. Nordström, Investigation of acceleration effects on missile aerodynamics using Computational Fluid Dynamics, *Aerospace Science and Technology* (2009), doi: 10.1016/j.ast.2009.04.008

Investigation of acceleration effects on missile aerodynamics using Computational Fluid Dynamics

I. M. A. Gledhill[1], K. Forsberg[2] , P. Eliasson [2], J. Baloyi[1], and J. Nordström [2,3]

[1]*DPSS, CSIR, PO Box 395, Pretoria 0001, South Africa*

[2]*FOI, Swedish Defense Research Agency, SE-164 90, Stockholm, Sweden*

[3]*Uppsala University, Department of Information Technology, SE-75105, Uppsala, Sweden and KTH, Department f Aeronautical and Vehicle Engineering, SE-10044, Stockholm, Sweden*

Abstract

In this paper we describe the implementation and validation of arbitrarily moving reference frames in the block-structured CFD-code EURANUS. We also present results from calculations on two applications involving accelerating missiles with generic configurations. It is shown that acceleration affects wave drag significantly. Also, it is shown that strake-generated vortices move significantly in turns. These results clearly show the necessity of including the acceleration effects in the calculations.

Keywords: acceleration, aerodynamics, drag, CFD, vortex

I. Introduction

In the past, CFD has largely been restricted to constant velocity objects with time-dependant models of transient phenomena, and to systems rotating with constant angular velocity such as atmospheric flows, turbines and rotating blades. The relative movement of subsystems has been included, in for example aeroelastic models, moving control surfaces, helicopter blades and store release. However, in order to be able to predict the behaviour of accelerating and manoeuvring flying bodies correctly, one must be able to treat arbitrarily moving reference frames.

Typical applications that prompted the development of this work include missile aerodynamics and the calculation of dynamic derivatives. It may be noted that fourth generation missiles execute turns at angular accelerations of the order of 10 *g* to 100 *g*, where *g* is the acceleration due to gravity. Interest is also being expressed in projectiles which are subjected to thrusts of the order of 100 *g* to 500 *g*. It is expected that significant changes in the flow field may result from acceleration of these magnitudes.

Basic theory which has been developed for dynamic derivatives under geometrical and speed constraints is well known (see, for example, Nielsen [1]). Early aerodynamic characterisation of spinning kinetic energy projectiles was carried out by Weinacht and Sturek [29]. Roll, yaw and pitch damping derivatives have been calculated by Cormier *et al.* [3] using quasi-stationary ALE (Arbitrary-Lagrangian-Eulerian) models [12]. ALE methods also proved useful in the calculation of the aerodynamic loads and roll-averaged pitch generated by canard dither in a simulation on multi-level Cartesian grids by Murman *et al.* [19]. The approach of using automatic differentiation to calculate dynamic derivatives has been used by Park *et al.* [23], [22], and Green *et al.* [10] tested low-order panel methods with automatic differentiation to obtain dynamic derivatives for the F-16XL aircraft. An alternative method through the reduced-frequency method of Murman [18] is appropriate for modelling forced oscillations. CFD solutions for oscillating blades, as encountered in helicopter forward flight, has been undertaken by a number of authors (*e.g.* Shaw and Qin [26]) and is frequently modelled by elastic deformation of the grid.

The aerodynamics of objects accelerating on arbitrary prescribed or 6DOF trajectories have also been modelled on overset or adaptive grids (for example, those quoted by Cenko *et al.* [2]), a method frequently applied to store separation in the transonic regime. For transonic missiles executing turns at 50 *g* to 100 *g*, however, the trajectory corridor covered by the store would require a background grid hundreds of metres in extent, making these methods practicable only for near-field interactions. Some work on linear acceleration has been performed by Roohani and Skews [25]. Extended trajectories have been obtained by the alternative method of integrating through the substantial databases that have been accumulated in aerodynamic parameter studies (*e.g.* Murman *et al.* [20]) but this can only be accomplished if the population of parameter space is sufficiently dense.

In contrast to the methods described above, the aim of this work is to allow the direct prediction of loads in *arbitrary* manoeuvres which may involve varying angular acceleration (as in the commencement or termination of a turn), and/or significant linear acceleration or thrust. Models of forced oscillations, or calculation of dynamic derivatives, are a subset of the desired capabilities.

II. Theory

A mathematical tool box for the analytic treatment of non-stationary problems with relatively moving frames, including an extended vector analysis in an arbitrary number of dimensions, has been formulated by Löfgren [17], and forms the foundation for the following finite volume formulation. Consider a fixed, inertial reference frame Σ, referred to as the absolute frame (Figure 1). Consider also a moving reference frame Σ′, which may be accelerating in an arbitrary fashion, and which is referred to as the relative frame.

Notation is introduced to distinguish between vectors in Σ viewed in Σ', and *vice versa*. A general vector a, with components in Σ viewed in Σ, is denoted by $\breve{a}$ when viewed from Σ'. For example, if a is constant in time but Σ' rotates, $\breve{a}$ must have rotating components. A vector $\underline{a}$ in Σ' is expressed as $\hat{\underline{a}}$ when viewed from Σ. The rotation of Σ' relative to Σ is denoted by the orthogonal transform U. Then

$$\hat{\underline{a}} = U \cdot \underline{a}, \quad \breve{a} = U^{-1} \cdot a = U^{t} \cdot a, \quad \det(U) = +1 \tag{1}$$

Let ***r*** be the displacement vector of the origin of Σ′ interpreted in Σ. Coordinates $\underline{x}$ in Σ′ are related to coordinates x in Σ by the transformation

$$x = r + \mathrm{U} \cdot \underline{x} \tag{2}$$

and its inverse. For time derivatives we are able [7] to define a rotation vector ω by

$$\omega \times (U \cdot \underline{a}) = \frac{\partial U}{\partial t} \cdot \underline{a} \tag{3}$$

Differentiating with respect to time we obtain absolute and relative velocities respectively:

$$\begin{aligned} v &= \dot{r} + U \cdot (\underline{v} + \breve{\omega} \times \underline{x}) = \dot{r} + \hat{\underline{v}} + \breve{\omega} \times \underline{x} \\ \underline{v} &= -\dot{r} + \breve{v} - \breve{\omega} \times \underline{x} \end{aligned} \tag{4}$$

The relative velocity field $\underline{u}$ between the two frames is defined by $\underline{u} = \breve{v} - \underline{v}$ which leads to

$$\dot{\underline{u}} = \dot{\breve{r}} + \breve{\omega} \times \underline{x} \tag{5}$$

Spatial derivatives and frame transformations can then be derived [7]. Note that density and pressure are invariant under transformation. The conservation equations may be expressed in Σ or Σ′. Conventionally, CFD calculations are carried out in the relative frame Σ′. The coordinate system and grid attached to the object in Σ′ are shown in fig. 1. To illustrate the formulation, in the absolute frame we have

$$\frac{\partial}{\partial t}\int_V \rho v dV + \oint_{\partial V} (\rho v \otimes (v - \underline{\hat{u}}) + pI) \cdot d\underline{\hat{S}} = 0 \tag{6}$$

where the tensor product with components $[a \otimes b]_{ij} = a_i b_j$ has been used and viscous fluxes have been neglected for the purposes of illustration. In the relative frame, it is possible to show that the momentum conservation equation can be written [7]

$$\frac{\partial}{\partial t}\int_V \rho \underline{v} dV + \oint_{\partial V} (\rho \underline{v} \otimes \underline{v} + pI) \cdot d\underline{S} = -\int_V \rho \left(\frac{\partial \breve{\dot{r}}}{\partial t} + \frac{\partial \breve{\omega}}{\partial t} \times \underline{x} + 2\breve{\omega} \times \underline{v} + \breve{\omega} \times (\breve{\omega} \times \underline{x})\right) dV \tag{7}$$

The complicated source terms in the non-inertial frame can be interpreted as the fictitious forces of Batchelor [1] and Greenspan [11]. From the left, the terms represent the fictitious forces of translational acceleration (if U captures all rotation), angular acceleration, Coriolis effects, and centrifugal effects in the non-inertial frame. In the absolute frame Σ, no source terms appear.

In a numerical implementation, there is a choice between using the absolute frame formulation and the absolute velocities $\boldsymbol{v}$ or the relative frame formulation and velocities $\underline{\boldsymbol{v}}$. The relative velocities $\underline{\boldsymbol{v}}$ are small close to solid bodies for viscous calculations where the grid tends to be very fine. Hence, they reduce the risk of inaccuracies arising from truncation error. The presence of significant source terms, however, may change the properties of the numerical scheme and the conservative character is lost.

The absolute formulation and the use of absolute velocities $\boldsymbol{v}$ can be integrated very easily into schemes which already use stretchable coordinates or moving grids. Modifications are required to boundary conditions, and since absolute velocities $\boldsymbol{v}$ are frequently difficult for practitioners to interpret, the transformation of flow fields to the relative frame is a necessary tool. An estimate indicates that truncation errors in the near field would be acceptably reduced by the use of double precision. The absolute formulation was therefore chosen for the present work. A precise description

of the computational procedure is given in Forsberg [7], and related background material can be found in previous papers [8], [9].

III. Implementation

For the numerical implementation we have used EURANUS, which is a general Euler and Navier-Stokes solver for structured, and possibly non-matching, multi-block meshes. A cell centred finite volume approach is used with central differences, symmetric Total Variation Diminishing (TVD) or upwind TVD flux difference splitting. An explicit Runge-Kutta local time-stepping is used for steady state calculations, and an implicit time-integration with dual time-stepping is used for the time accurate computations. To enhance the convergence implicit residual smoothing (IRS) and full approximation storage (FAS) multigrid are used.

EURANUS already has grid-stretching introduced for aero-elastic purposes which greatly simplify the introduction of moving reference frames. This code is extensively verified ([24], [5], [15], [6], [28]). The existing routines supporting the implementation of stretchable meshes for aero-elastic calculations made the implementation of absolute instead of relative velocities straightforward. No extra terms which might ruin the conservative form of the equations have been added [5]. The modifications to the boundary condition routines and the rest of the program required by the presence of absolute velocities were also found to be minor.

The input variables are $\underline{\dot{r}}$, the velocity of the Σ' origin seen in Σ', and $\underline{\omega}$, the rotation of the moving frame about its origin, seen in Σ'. Input is provided by the user at arbitrary successive times in the input file. Cubic interpolation then provides values at intermediate times corresponding to the solver time steps. Although the implementation is fully viscous only Euler cases are shown in this paper.

IV. Validation case 1: rotating plate

In order to validate the implementation of the rotation transform, the existing extensively verified version of EURANUS intended for coordinate systems rotating with constant angular velocity has been used for comparison. This version includes rotation effects as source terms on the right-hand side of

the Navier-Stokes equations. From this point in the paper, variables are written without the frame notation in Σ'.

As a simple test case incorporating the steady revolution of a simple flat plate of zero thickness is constructed and rotated about a centre at distance *R (*see Figure 2). The circular trajectory is followed by a pivot point either halfway along the plate (centre case) or at the leading edge of the plate (skew case). The revolution angular velocity is 40 s^{-1}, the revolution radius 5 m and the speed of the plate 200 ms^{-1}. A comparison between the pressures on the plate for the two cases is shown when convergence has been reached in Figure 3. No significant differences between the results are seen.

V. Validation case 2: constant velocity airfoil

The simplest validation for linear velocity terms to be performed is a test of Galilean invariance with no frame acceleration present, in which the pressure profile across an airfoil travelling at constant velocity ($-u_x, -u_y, 0$), modelled in the absolute frame with stagnant far-field boundary conditions, is compared with the pressure profile across an airfoil modelled in the relative frame with free stream boundary conditions ($u_x, u_y, 0$). No acceleration is present in these cases.

The conditions chosen are Mach 0.8 with angle of attack α = 1.25º. A two-dimensional grid with 257 x 65 points is used. The chord length L is 1.0 m; characteristic far field boundaries are placed at 25 chord lengths away from the slip airfoil surface in the dimensions modelled. A second order central difference scheme was used with Jameson dissipation [14], [13]. An implicit five stage Runge-Kutta scheme with backward Euler time differencing, 5 W-cycle multi-grid levels and residual smoothing were used. Pressure coefficients C_p were compared for relative and absolute frames and are very similar for the two cases.

VI. Validation case 3: oscillating airfoil

We consider the oscillating airfoil case published by Landon [16]. The experimental pressure and force measurements have been extensively used to evaluate time-dependant solvers [30], [4]. The entire grid oscillates rigidly and the grid moves at Mach 0.755. At far-field boundaries, conditions of

stagnant flow (zero velocity) are imposed. The angle of attack of the airfoil varies as a function of time t as

$$\alpha(t) = \alpha_0 + \alpha_1 \sin \omega t \tag{8}$$

with α_0 = 0.016º and α_1 = 2.51º. The angular velocity ω is chosen such that the dimensionless frequency k = 0.0814, with the definition $k = \omega L / 2u_\infty$ where L is the scale length, in this case the chord length, and u_∞ is the relative speed of the airfoil and the flow. The airfoil is oscillated about its quarter-chord point. A two-dimensional O-mesh with 129 points on the airfoil surface and 33 points to the outer boundary was used [27].

The chord length is 1.0 m (in contrast to that of Landon [16], where the chord length in the experiment was 0.1016 m). Characteristic far field boundaries are placed at 25 chord lengths away from the airfoil, and the external flow is specified as stagnant. In the absolute frame, the airfoil is moved at speed $u = -u_\infty$ and pitched so that the angle of attack is given by equation (6). A steady field for α_0 = 0.016º was provided as initialisation.

The normal force coefficients C_N and pitching moment C_m are shown as a function of α in Figure 4, and pressure coefficients C_p for selected α are shown in Figure 5. The agreement between the absolute frame model and experimental results is reasonable and consistent with other calculations [10].

VII. Application case: rapidly accelerating missile

As a first application, we consider a simple missile configuration with a flare subject to very rapid (4500 ms^{-2}) linear acceleration along the major axis (Figure 6). At these extreme accelerations no experiments are yet available. The main practical interest is in the impact of the acceleration on the drag coefficient C_d. We compare with steady state calculations performed at a given set of velocities.

The results of Euler calculations for the simplified missile are shown in Figure 7. The drag coefficient has been normalized with respect to the instantaneous dynamic pressure. The main observed impact of the acceleration on the drag is that the transonic maximum is reduced by

approximately 20% and moved above the speed of sound, having a maximum value at approximately Mach 1.2.

VIII. Application case: vortex behaviour in turn

A motivating interest application is the increasing manoeuvrability of missiles. As illustrated in Figure 8, vortices from nose, canards, body or strakes which interact with fins may move as a result of significant acceleration in a turn, and at certain angles of attack may change either fin disruption or pressure footprints on the body. The vortices in this case are generated along sharp-edged zero-thickness strakes rather than by separation along the curved surfaces of the hemisphere-cylinder body, Figure 9.

For a typical speed of 600 ms^{-1}, a pitch rate of q=1 s^{-1} corresponds to a turn radius of 60 m, and a transverse acceleration of 600 ms^{-2} or approximately 60 g, where g is the acceleration due to gravity. For a 2 m typical length L, the ratio of L to turn radius R is about 1/30, indicating that centrifugal effects would be small but significant. The Rossby number U/2Lq is 150.

The total length is 2.000 m, the diameter is 0.100 m, and the strakes project 0.010 m from the surface. The origin is at the nose of the hemisphere and the coordinate x extends along the main axis. We define the angle of attack α as the kinematic angle between the direction of flow and the x axis in the body axis system, and the pitch angle θ as the attitudinal angle between a fixed axis in an inertial system, which may be referred to as x_I, and the x axis in the body axis system. The pitch rate or angular velocity, q, is defined as $\dot{\theta}$. The object executes a circle with α constant and constant q. From derivatives with respect to q of the pitching moment C_m and the lift coefficient C_N we obtain the dynamic derivatives C_{mq} and C_{Nq} respectively.

Normal force coefficients and pitching moment coefficients for varying q are shown in Figure 10 for α = 15º. Lines have been fitted to the points excluding q < -10 s^{-1} and the dynamic derivatives $C_{mq} = \partial C_m/\partial q$ and $C_{Nq} = \partial C_N/\partial q$ are the slopes.

We compare the flow field at α = 15º and no rotation, q = 0 s^{-1}, with the flow field for a sample rotation, q = -5 s^{-1}. The upper strake vortices can easily be traced from their inception and their

propagation backwards until they eventually merge with the wake. To quantify the pressure change, we consider the difference field $\Delta p = p|_{q=-5} - p|_{q=0}$.

In the wake, a clear displacement exists in the top strake vortex under rotation, and the displacement is upwards, towards the centre of revolution; the contrast appears in Figure 11 (a) and (b) at x = 2.5 m. The difference field Δp shows changes of the order of 10^4 Pa. The pressure changes on the windward side of the body account for the dominant contribution to lift and pitching moment with negative q in Figure 10.

IX. Conclusions

We develop and implement a prediction method applicable to the aerodynamics of arbitrary manoeuvres, formulated in the absolute frame. The absolute frame formulation has the advantage that no source terms need be incorporated, and conservation is automatic. The method was easy to implement in the existing well-validated Navier-Stokes code EURANUS, since partly-moving meshes have already been incorporated for aeroelastic purposes. We have validated the absolute frame method using pressure coefficients over a constant velocity transonic NACA0012 test case, a rotating plate and the oscillating airfoil data of Landon [16].

A flare has been accelerated through Mach 1 and the drag coefficient results compared with those obtained at constant velocity. The main observations that the transonic maximum wave drag is reduced by approximately 20% and that the maximum value occurs at approximately Mach 1.2. To investigate the effect of turn rate, we considered vortices being generated along sharp-edged strakes on a hemisphere-cylinder. In the wake, a clear displacement exists in the top strake vortex under rotation towards the centre of revolution. These effects are of interest because vortices from nose, canards, body or strakes which interact with fins will move as a result of significant acceleration in a turn, and at certain angles of attack may change either fin disruption or pressure footprints on the body. Also, the dynamic derivatives C_{mq} and C_{Nq} are easily available from the method.

Acknowledgments

The authors wish to thank all colleagues at both participating institutions, and particularly Ola Hamner for his part in suggesting the problem, and Hannes van Niekerk for support in South Africa.

The project support of CSIR (Defence, Peace, Safety and Security Unit) and Department of Defence, South Africa, and the support of SIDA (Swedish International Development Authority) and the NRF (National Research Foundation, South Africa) in exchange visits, is gratefully acknowledged.

References

[1] G.K. Batchelor, An Introduction to Fluid Dynamics, Cambridge University Press, Cambridge, 1967.

[2] A. Cenko, D. Gowanlock, M. Lutton, M. Tutty, F/A-18C/JDAM Applied Computational Fluid Dynamics Challenge II results, AIAA-2000-0795 (2000).

[3] J. Cornier, S. Champagneux, V. Moreuxt, R. Collercandy, Prediction of quasi-stationary aerodynamic coefficients using the ALE method, in: ECCOMAS 2000, Barcelona, Spain, 2000.

[4] P. Eliasson, J. Nordström, The development of an unsteady solver for moving meshes, FFA, The Aeronautical Research Institute of Sweden, FFA TN 1995-39 (1995).

[5] P. Eliasson, J. Nordström, L. Torngren, L. Tysell, A. Karlsson, B. Winzell, Computations and Measurements of Unsteady Pressure on a Delta Wing with an Oscillating Flap, Proc. 3rd ECCOMAS CFD Conf., Paris, Wiley, (1996), pp. 478-484.

[6] P. Eliasson, D. Wang, S. Meijer, J. Nordström, Unsteady Euler Computations through Non-Matching and Sliding-Zone Interfaces, AIAA-98-0371 (1998).

[7] K. Forsberg, Treatment of a moving reference frame for discretised NS equations, FFA-TN, Flygtekniska Försöksanstaleten, The Swedish Aeronautical Institute, 2000.

[8] K. Forsberg, I.M.A. Gledhill, P. Eliasson, J. Nordström, Investigations of Acceleration Effects on Missile Aerodynamics using CFD, AIAA-2003-4084 (2003).

[9] I.M.A. Gledhill, J. Baloyi, M. Maserumule, K. Forsberg, P. Eliasson, J. Nordström, Accelerating systems: some remarks on pitch damping, in: 5th SA Conference on Computational and Applied Mechanics, Cape Town (2006) pp. 268-275.

[10] L.L. Green, A.M. Spence, P.C. Murphy, Computational methods for dynamic stability and control derivatives, AIAA 2004-0015 (2004).

[11] H.P. Greenspan, The Theory of Rotating Fluids, Cambridge University Press, Cambridge, 1968.

[12] C.W. Hirt, A.A. Amsden, J.L. Cook, An Arbitrary-Lagrangian-Eulerian computing method for all flow speeds, J. Computational Physics, 14 (1972) 227-254.

[13] A. Jameson, Transonic airfoil calculations using the Euler equations, in: P. L. Roe, ed., Numerical Methods in Aeronautical Fluid Dynamics, New York, Academic Press, 1982.

[14] A. Jameson, W. Schmidt, E. Turkel, Numerical simulation of the Euler equations by finite-volume methods using Runge-Kutta time stepping schemes, AIAA-81-1259 (1981).

[15] A. Karlsson, B. Winzell, P. Eliasson, J. Nordström, L. Torngren, L. Tysell, Unsteady Control Surface Pressure Measurements and Computations, AIAA-96-2417 (1996).

[16] R.H. Landon, NACA 0012 Oscillating and Transient Pitching, Compendium of Unsteady Aerodynamic Measurements, Data Set 3, AGARD-R-702, 1982.

[17] P. Löfgren, Relative motion in fluid mechanics, FFAP-B-066, Flygtekniska Försöksanstaleten, The Swedish Aeronautical Institute, 1988.

[18] S.M. Murman, A reduced-frequency approach for calculating dynamic derivatives, AIAA-2005-0840 (2005).

[19] S.M. Murman, S.J. Aftosmis, M.J. Berger, Numerical simulation of rolling airframes using a multi-level Cartesian method, AIAA-2002-2798 (2002).

[20] S.M. Murman, M.J. Aftosmis, M. Nemec, Automated parameter studies using a Cartesian method, NAS Technical Report, NAS-04-015 (2004).

[21] J.N. Nielsen, Missile Aerodynamics, Nielsen Engineering & Research, Inc., California, 1988.

[22] M.A. Park, L.L. Green, Steady-state computation of constant rotational rate dynamic stability derivatives, AIAA-2000-4321 (2000).

[23] M.A. Park, L.L. Green, R.C. Montgomery, D.L. Raney, Determination of stability and control derivatives using computational fluid dynamics and automatic differentiation, AIAA 1999-3136 (1999).

[24] A. Rizzi, P. Eliasson, I. Lindblad, C. Hirsch, C. Lacor, J. Häuser, The Engineering of Multiblock/Multigrid Software for Navier-Stokes Flows on Structured Meshes, Computers and Fluids, 22 (1993) 341-367.

[25] H. Roohani, B.W. Skews, Investigation of the effects of acceleration on aerofoil aerodynamics, in: 5th SA Conference on Computational and Applied Mechanics, Cape Town (2006) pp. 260-267.

[26] S.T. Shaw, N. Qin, Study of the aerodynamics of in-plane motion, J. Aerospace Engineering, 215 (2001) 89-104.

[27] L.G. Tysell, S.G. Hedman, Towards a general three-dimensional grid generation system, ICAS 88-4.7.4, (1988).

[28] D. Wang, S. Wallin, M. Berggren, P. Eliasson, A computational study of the unsteady turbulent buffet aerodynamics, AIAA-2000-2657 (2000).

[29] P. Weinacht, W.B. Sturek, Computation of the roll characteristics of finned projectiles, U S Army Laboratory Command Technical Report BRL-TR-2931 (1988).

[30] W. Woodrow, M. Hafez, S. Osher, An entropy correction method for unsteady full potential flows with strong shocks, AIAA-86-1768 (1986).

Figure 1: Fixed, or absolute, frame Σ, and moving, or relative, frame Σ′.

Figure 2: Rotating plate geometry with rotation centre at (a) plate centre and (b) leading edge

Figure 3: Comparison of relative and absolute frame pressure for rotating plate with rotation centre at (C) plate centre and (LE) plate leading edge

Figure 4: (a) Normal force coefficient and (b) Pitching moment coefficient for experimental results [16] and absolute frame model with 96 time steps per cycle.

Figure 5: Pressure coefficient as a function of *x*; upper surface experimental data [16] shown as solid circles on upper surface and circles on lower surface

Figure 6: Flare geometry, measurements in mm

Figure 7: Drag coefficient results for Euler calculations, normalised with respect to instantaneous dynamic pressure, for steady state flare (solid circles) and linearly accelerated flare (crosses and line).

Figure 8: Schematic illustration of vortices (shaded) in (a) constant velocity flight and (b) turn

Figure 9: Geometry of straked body

Figure 10: Normal force coefficients C_N (solid symbols) and pitching moment coefficients C_m (open symbols) in the relative frame for $\alpha = 15^o$ with fitted lines

Figure 11: Contours of pressure for $\alpha = 15^o$, $x = 2.5$ m, $q = 0$ s^{-1} (a) and $q = -5$ s^{-1} (b). Contours are drawn at the same intervals in each case. The horizontal red line represents y = 0 m. The difference field is shown in (c).

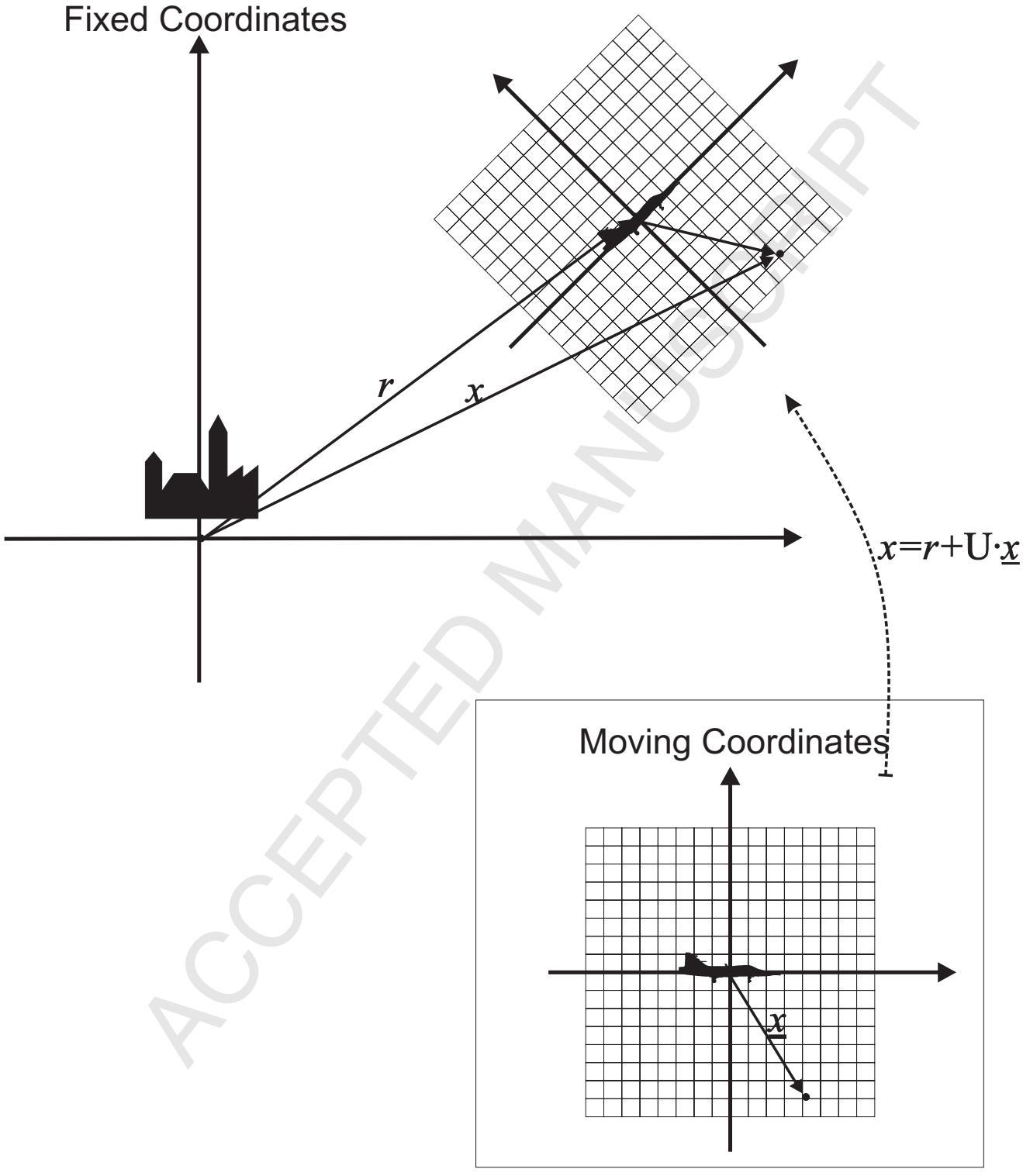

fig1

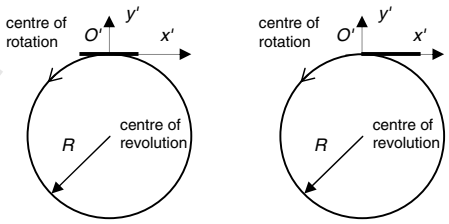

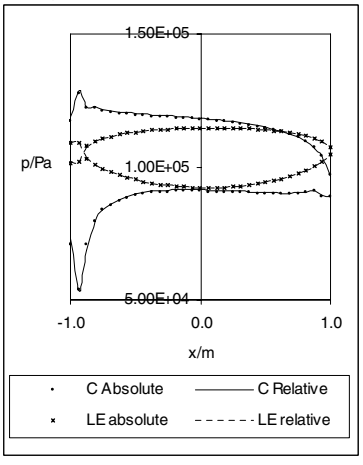

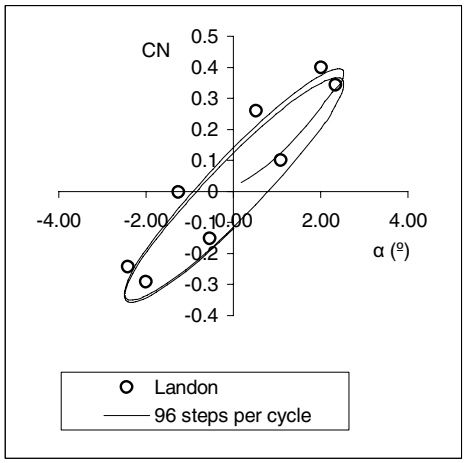

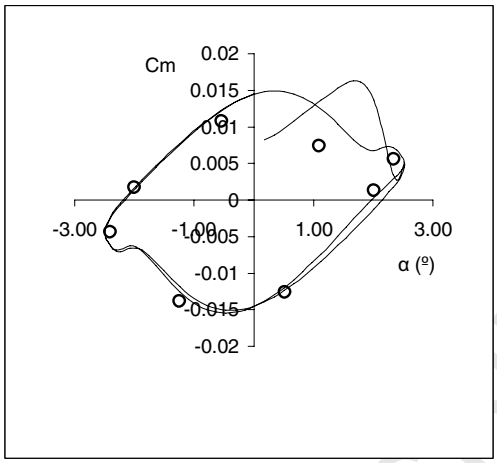

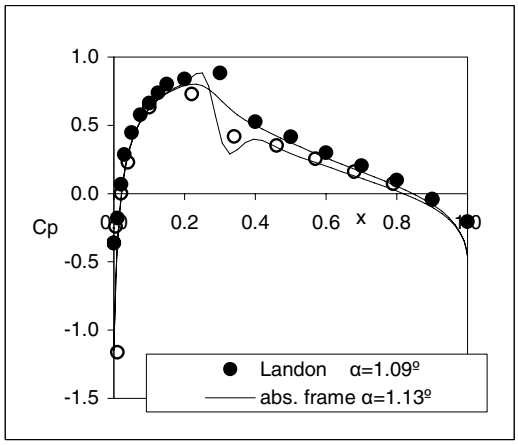

(a)

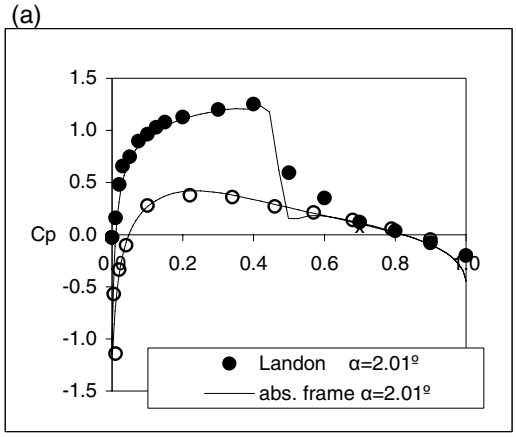

(b)

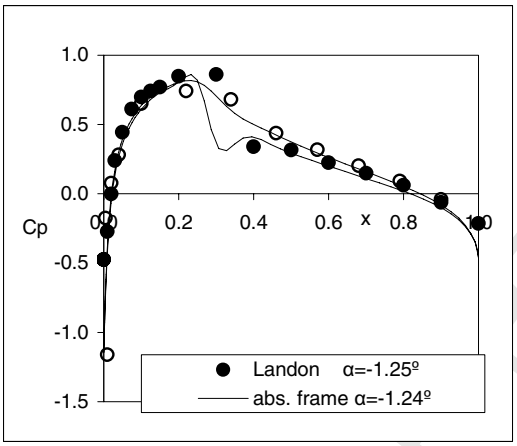

(c)

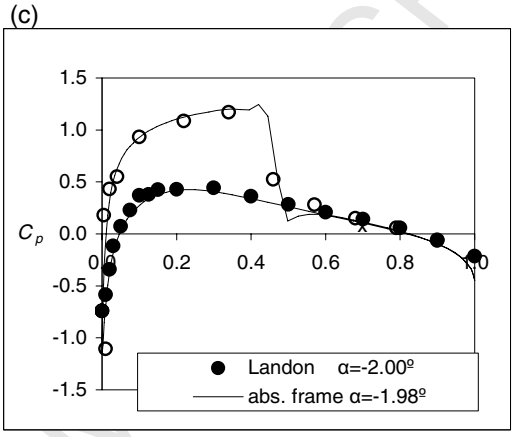

(d)

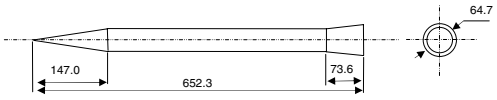

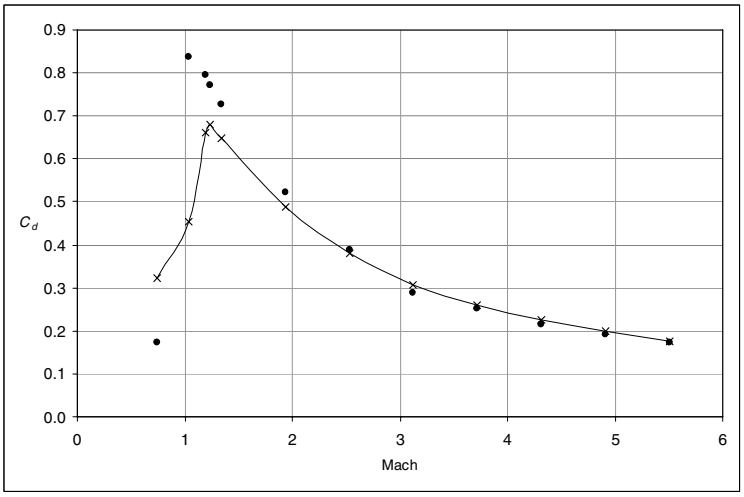

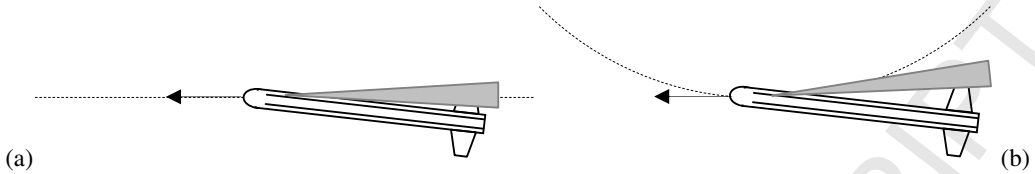

(a) (b)